Flexural Strengthening of Two-Way RC Slabs with Textile-Reinforced Mortar: Experimental Investigation and Design Equations

Lampros N. Koutas, Ph.D., Aff.M.ASCE[1]; and Dionysios. A. Bournas, Ph.D.[2]

Abstract: The application of textile-reinforced mortar (TRM) as a means of increasing the flexural capacity of two-way reinforced concrete (RC) slabs is experimentally investigated in this study. The parameters examined include the number of TRM layers, the strengthening configuration, the textile fibers material (carbon versus glass), and the role of initial cracking in the slab. For this purpose six large-scale RC slabs were built and tested to failure under monotonic loading distributed at four points. It is concluded that TRM increases substantially the precracking stiffness, the cracking load, the postcracking stiffness, and eventually the flexural capacity of two-way RC slabs, whereas the strengthening configuration plays an important role in the effectiveness of the technique. Simple design equations that provide good estimation of the experimental flexural moment of resistance are proposed. **DOI: 10.1061/(ASCE)CC.1943-5614.0000713.**

Author keywords: Flexural strengthening; FRCM; Reinforced concrete; Textile-reinforced mortar (TRM); Two-way slabs.

Introduction and Background

Strengthening of existing concrete structures has become an urgent need in recent years as a result of aging and/or the necessity to comply with the requirements of modern design codes (i.e., Eurocodes). As the main objective of strengthening methods is to achieve sustainability and cost-effectiveness, the engineering community has progressively turned to the use of advanced structural materials. The introduction of textile-reinforced mortar (TRM) almost a decade ago (Triantafillou et al. 2006; Bournas et al. 2007) can be recognized as remarkable progress in the field of structural retrofitting.

TRM is a cement-based composite material that consists of high-strength fibers (i.e., carbon, glass, or basalt) in the form of textiles combined with inorganic matrices, such as cement-based mortars. The textiles that are used as reinforcement of the composite material typically comprise fiber rovings in two orthogonal directions. The same material can also be found in the literature with the acronyms TRC or FRCM (e.g., Brameshuber 2016; ACI 2013; Carloni et al. 2015). One of the characteristics of TRM is its advantages over fiber-reinforced polymers (a broadly used epoxy-based composite material), namely, low cost, resistance at high temperatures, compatibility with concrete and masonry substrates, ability to apply on wet surfaces, and low temperatures and air permeability.

[1]Postdoctoral Research Associate, Dept. of Civil and Structural Engineering, Univ. of Sheffield, Sir Frederick Mappin Bldg., Mappin St., Sheffield S1 3JD, U.K.; formerly, Research Fellow, Faculty of Engineering, Univ. of Nottingham, Nottingham NG7 2RD, U.K. E-mail: L.Koutas@sheffield.ac.uk; koutasciv@gmail.com

[2]Research Officer, European Commission, Joint Research Centre (JRC), Institute for the Protection and Security of the Citizen (IPSC), European Laboratory for Structural Assessment, TP480, via Enrico Fermi 2749, I-21020 Ispra, Italy (corresponding author). E-mail: Dionysios.Bournas@jrc.ec.europa.eu

Note. This manuscript was submitted on November 24, 2015; approved on March 9, 2016; published online on June 30, 2016. Discussion period open until November 30, 2016; separate discussions must be submitted for individual papers. This paper is part of the ***Journal of Composites for Construction***, © ASCE, ISSN 1090-0268.

A significant research effort has been made in the last few years toward the exploitation of the TRM strengthening technique in several cases of structural retrofitting. Experimental investigations on strengthening of reinforced concrete (RC) (e.g., Bournas et al. 2009; Bournas and Triantafillou 2011; D' Ambrisi and Focacci 2011; Elsanadedy et al. 2013; Babaeidarabad et al. 2014; Koutas et al. 2014; Tzoura and Triantafillou 2014; Bournas et al. 2015; Loreto et al. 2015; Ombres 2015; Tetta et al. 2015, 2016) or masonry elements (Papanicolaou et al. 2007; Harajli et al. 2010; Babaeidarabad et al. 2013; Koutas et al. 2015a, b) have shown very promising results. Research on strengthening of RC slabs, though, has been rather limited (Jesse et al. 2008; Papanicolaou et al. 2009; Schladitz et al. 2012; Loreto et al. 2014), with most of the studies focusing on the flexural behavior of one-way slabs. The only study reported in the international literature on strengthening of two-way RC slabs with TRM is that of Papanicolaou et al. (2009) who tested four square slabs under concentrated load with three of them being retrofitted with carbon or glass TRM. Nevertheless, all slabs in the study of Papanicolaou et al. (2009) (including the unretrofitted one) failed in punching shear without developing a plastic collapse mechanism in flexure, and therefore TRM served for a punching shear capacity increase.

The use of TRM for increasing the flexural capacity of two-way RC slabs has not been investigated to date. This paper investigates for the first time the flexural strengthening of two-way RC slabs with externally bonded TRM. The parameters under investigation are the number of TRM layers, the strengthening configuration, the material of the textile fibers, and the presence of initial cracking. For this purpose, six large-scale slabs were experimentally tested, with the results being used to derive simple design equations. Details are provided in the following sections.

Experimental Program

Test Specimens and Parameters

The experimental program aimed to study the effectiveness of externally bonded TRM in increasing the flexural capacity of

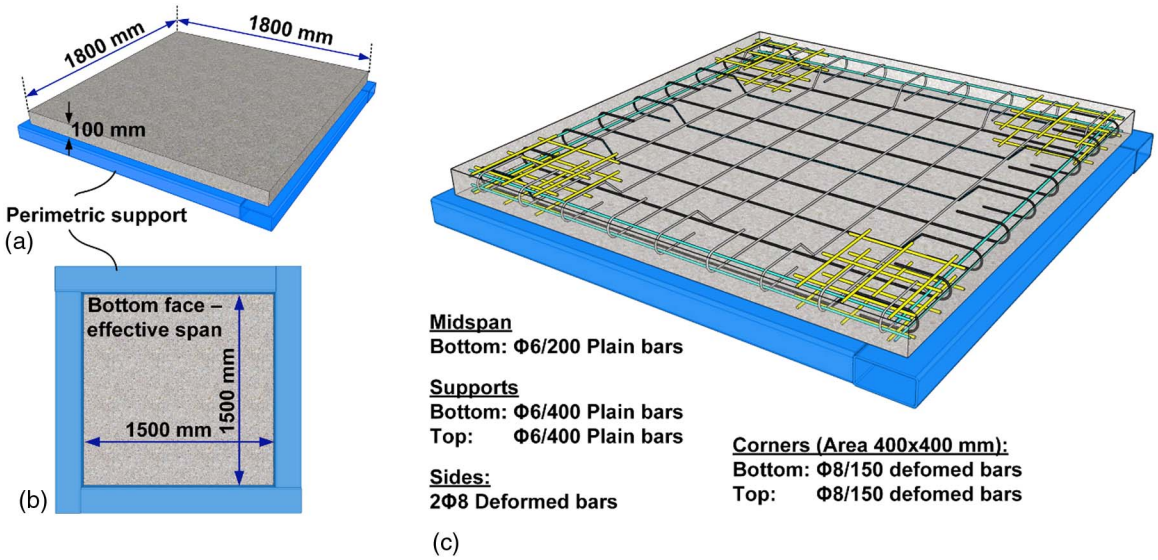

Fig. 1. (a) Geometry of the slab; (b) bottom face of the slab supported in its perimeter; (c) steel reinforcement details and 3D visualization

two-way RC slabs. Six slabs with the same geometry were constructed and tested as simply supported at their perimeter (Fig. 1). As shown in Fig. 1(a), the slabs had a length of 1,800 mm on both sides (square slabs) and a thickness of 100 mm, whereas the effective flexural span was 1,500 mm [Fig. 1(b)]. The slabs' geometry represented a prototype slab at a scale of ½.

All slabs were lightly reinforced with plain steel bars ($\rho_s = 0.17\%$) so as to have low flexural capacity, simulating flexure-deficient slabs (i.e., corrosion of rebars; increase of slab loading). Details of the reinforcement are shown in Fig 1(c). Plain steel bars with a 6 mm-diameter and a spacing of 200 mm were placed at the bottom of the midspan in both directions. Half of them were bent at a distance of 300 mm from the edge and continued toward the support as top reinforcement. All plain bars were bent over 180 degrees at their ends to ensure proper anchorage. Extra grid reinforcement (consisting of 8-mm-diameter deformed bars) was placed at the four corners to avoid cracking as a result of twisting moments.

The role of various parameters on the effectiveness of TRM strengthening schemes was investigated, namely, the number of TRM layers, the material of the fibers (carbon versus glass), the strengthening configuration (full coverage versus partial coverage), and the presence of initial damage (cracked versus uncracked). A description of the specimens follows, supported by Fig. 2 and Table 1:

- One slab (CON) was tested without strengthening and served as control specimen [Fig. 2(a)].
- Specimen C1 was strengthened with one layer of carbon textile, applied over the full tensile face [Fig. 2(b)].
- Specimen C2 was strengthened similarly to C1, applying two layers of carbon textile instead of one [Fig. 2(c)].
- Specimen C1_part received two strips of carbon textile in a cross configuration (one per direction) [Fig. 2(d)]. Each strip had a width equal to half of the effective span, resulting in half the amount of fibers per direction of application when compared to C1. Nevertheless, the total weight of the textile used in the C1_part was the same as in C1.
- Specimen G3 was strengthened with three layers of glass fiber textile, applied over the full tensile face of the slab. Three layers of glass textile are equivalent (in terms of axial stiffness) to 3/7 (approximately half) of one carbon textile layer [Fig. 2(e)].
- Finally, specimen C3_cr was strengthened with three layers of carbon textile applied over the full tensile face that was previously fully cracked [Fig. 2(f)].

All strengthening schemes were applied on the tensile face of the slabs.

Materials and Strengthening Procedure

Casting of the slabs was made in two groups on different dates by using ready-mix concrete. The average compressive strength on the day of testing the slabs, measured on cubes with dimensions of $150 \times 150 \times 150$ mm (average values from three specimens), is given for each specimen in Table 1. The 6-mm-diameter plain longitudinal bars had a yield stress of 470 MPa, a tensile strength of 508 MPa, and an ultimate strain of 7.2%. The respective values for the 8-mm-diameter deformed bars were 568 MPa, 654 MPa, and 11.5% (average values from three specimens).

A carbon textile was used as external reinforcement in four slabs, whereas a glass textile was used in one slab. The carbon textile [Fig. 3(a)] had a weight of 348 g/m^2 with uncoated (dry) carbon-fiber rovings in two orthogonal directions and an equal amount of fibers in each one. The resulting nominal thickness of this textile in each direction was 0.095 mm. According to the manufacturer data sheets the tensile strength and the modulus of elasticity of the carbon fibers were 3,800 MPa and 225 GPa, respectively. The glass textile [Fig. 3(b)] had a weight of 220 g/m^2 and equal amount of uncoated (dry) glass fibers in two orthogonal directions. The nominal thickness of this textile was 0.044 mm and according to the manufacturer data sheets the tensile strength and the elastic modulus of the glass fibers were 1,400 MPa and 74 GPa, respectively.

The mortar used as a binding material between the textile and the concrete substrate was a polymer-modified cement-based mortar with an 8:1 cement-to-polymers ratio by weight. The water-to-cementitious-material ratio by weight was equal to 0.23, resulting in plastic consistency and good workability. Table 1 includes the strength properties of the mortar (average values of three specimens) obtained experimentally on the day of testing using prisms with dimensions of $40 \times 40 \times 160$ mm, according to the EN 1015-11 (CEN 1999). The slightly different strength values between the two groups of specimens are attributed to a small difference in the age of tested slabs.

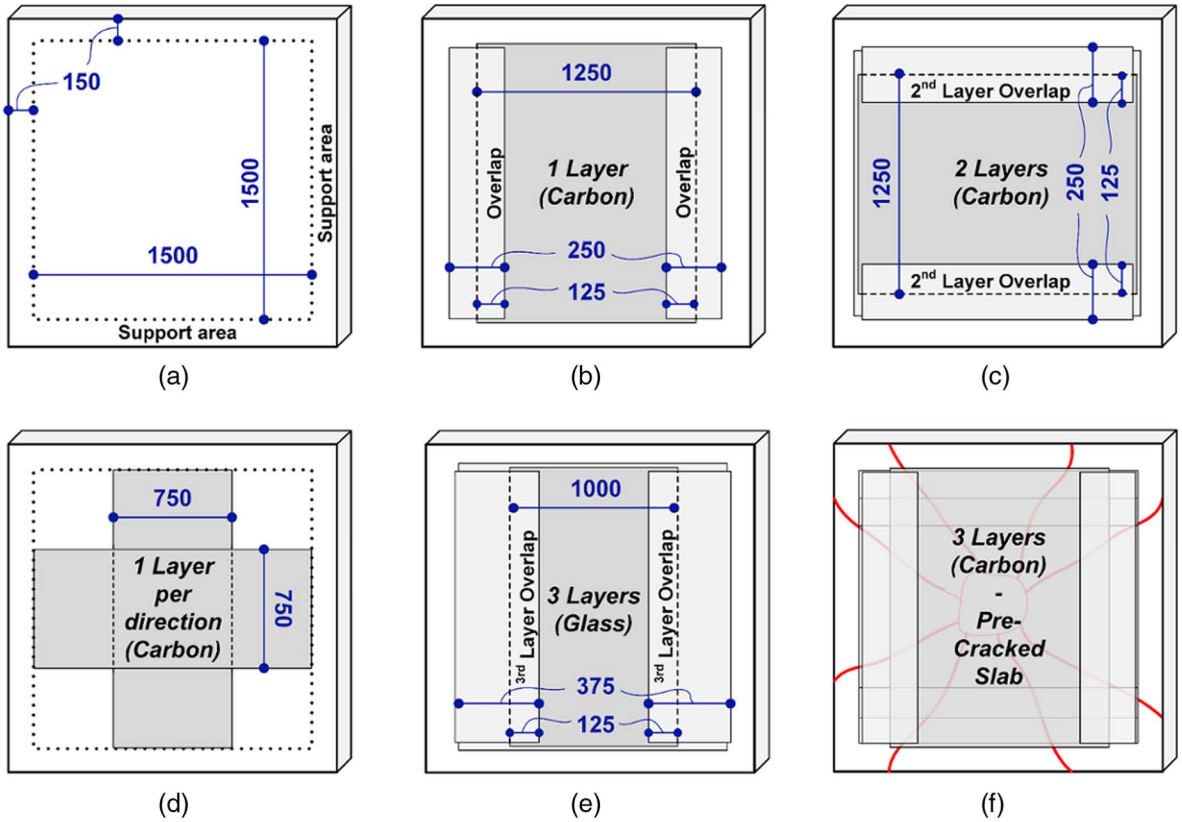

Fig. 2. Strengthening configuration at the tensile face of tested slabs (all dimensions in mm): (a) CON; (b) C1; (c) C2; (d) C1_part; (e) G3; (f) C3_cr

Table 1. Specimens, Experimental Parameters, and Materials

Specimen	Strengthening configuration	Steel reinforcement ratio, ρ_s (per direction) (%)	Textile reinforcement ratio, ρ_t (per direction)	Concrete compressive strength, f_c (MPa)	Mortar compressive strength, f_{mc} (MPa)	Mortar flexural strength, $f_{mt,fl}$ (MPa)
CON	—	0.17	—	19.8 (0.8)[a]	—	—
C1	One layer of carbon textile covering the full tensile face	0.17	0.095%	19.8 (0.8)[a]	33.1 (1.2)[a]	8.0 (0.3)[a]
C2	Two layers of carbon textile covering the full tensile face	0.17	0.19%	19.8 (0.8)[a]	33.1 (1.2)[a]	8.0 (0.3)[a]
C1_part	Two strips of carbon textile in cross configuration (one per direction), covering half of the tensile face	0.17	0.0475%	22.2 (0.5)[a]	36.6 (0.8)[a]	8.9 (0.4)[a]
G3	Three layers of glass textile covering the full tensile face	0.17	0.132%	22.2 (0.5)[a]	36.6 (0.8)[a]	8.9 (0.4)[a]
C3_cr[b]	Three layers of carbon textile covering the full tensile face	0.17	0.285%	22.2 (0.5)[a]	36.6 (0.8)[a]	8.9 (0.4)[a]

[a]Standard deviation in parenthesis.
[b]Strengthening was applied on a precracked slab.

The strengthening procedure included the following steps: (1) removal of a thin layer of concrete and formation of a grid of groves (2 mm deep) at the surface to receive strengthening [Fig. 4(a)], (2) dampening of the surface [Fig. 4(b)], (3) application of a first mortar layer (2 mm thick) by using a smooth metal trowel [Fig. 4(c)], (4) application of the first textile layer into the mortar by hand pressure [Fig. 4(d)], and (5) application of a second mortar layer to completely cover the textile. For the application of more layers the last two steps were repeated, while the previous layer was still in a fresh state.

In the cases where TRM covered the whole tensile face of the slab, each layer comprised three textile patches, which were overlapped at a length of 125 mm as illustrated in Fig. 2. For example, Fig. 4(e) shows the application of an extra patch to fully cover the tensile face of the slab strengthened with three layers of glass fiber textile. This is attributed to the fact that the textiles were manufactured into rolls of widths equal to 1,250 and 1,000 mm for the carbon and the glass fibers, respectively. Finally, a picture of a slab at completion of the strengthening application is shown in Fig. 4(f).

Test Setup and Procedure

All specimens were subjected to monotonic flexural loading and were tested as simply supported at their perimeter [Fig. 5(a)]. The load was applied at a displacement rate of 1 mm/min by using a 500-kN-capacity servohydraulic actuator that was mounted at a stiff steel reaction frame, as shown in Fig. 5(b).

The test specimen was laid on four rigid steel beams, which in turn were simply supported at four corners, as shown in Figs. 5(a and b). The effective flexural span in both directions was 1,500 mm. Geometrical imperfections of the wooden molds resulted in small

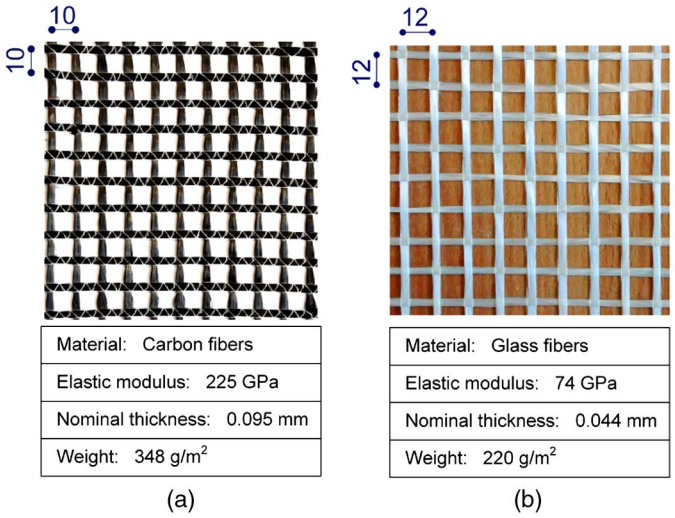

Fig. 3. Textiles used in this study: (a) carbon fibers; (b) glass fibers (dimensions in millimeters)

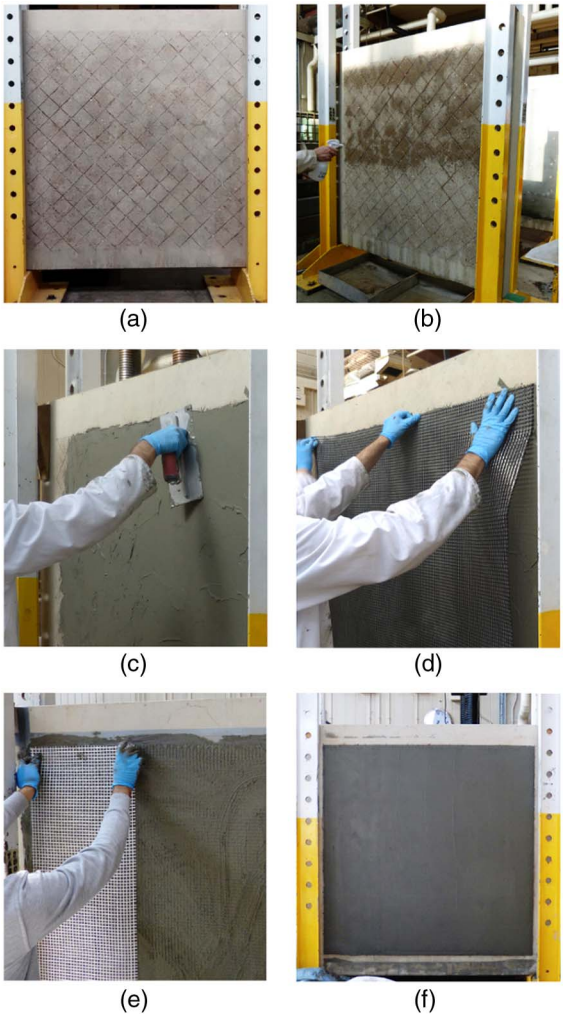

Fig. 4. TRM strengthening application steps: (a) concrete surface preparation; (b) dampening of surface to receive strengthening; (c) first mortar layer application; (d) carbon textile application; (e) patch of glass textile application; (f) final finished surface

gaps between the supports and the slabs in some regions over the perimeter. Therefore, a thin sand layer (approximately 10 mm) was placed between the support beams and the slabs to ensure full contact during the test. As illustrated in Fig. 5(a), a system of stiff steel beams was used to spread the load into four points; this helped to achieve a more uniform load distribution. The four load-application areas were centrally located, forming a grid 500 × 500 mm within the effective flexural span [Fig. 5(c)]. To avoid concentration of high local stresses in these areas, square rubber pads of dimensions 150 × 150 × 40 mm were placed in between the top of the slab and the stiff steel beams.

In addition to the internal LVDT (linear variable differential transformer) of the actuator, five potentiometers were installed at the bottom of the specimen in a cross configuration to measure the deflections in both bending directions [Fig. 5(d)]. Specifically, one potentiometer (POT1) was installed at the center of the slab and the other four at a distance of $L/4$ from POT1 in each direction (where L is the effective span). All data were synchronized and recorded using a data acquisition system.

Apart from C3_cr, all specimens were tested up to failure. Specimen C3_cr was first subjected to a load level where yielding of the steel reinforcement occurred (and significant cracking was observed), and then it was unloaded. It was finally tested up to failure after strengthening and curing.

Test Results

The responses of all slabs tested are presented in Fig. 6 in the form of load versus central deflection curves, whereas the final crack pattern of each slab is illustrated in Fig. 7. Table 2 also summarizes the main test results: the peak load, P_{max}; the midspan deflection corresponding to P_{max}; the observed failure mode; the flexural capacity increase from strengthening; the precracking (initial) stiffness, which is calculated from the force-midspan deflection curves as the tangent stiffness of the uncracked stage; the cracking load (approximate load level based on the observations during testing and the change in the slope of load-displacement curves); the postcracking stiffness, which is calculated from the force-central deflection curves as the tangent stiffness of the cracked state; and the load at the serviceability limit state (SLS). According to the Eurocode 2—Part 1 (CEN 2004), the SLS is reached when the midspan deflection becomes equal to $\ell/250$, where ℓ is the slab's effective span (here this deflection is equal to 6 mm).

As designed, the control slab (CON) failed in flexure after yielding of the steel reinforcement and the development of significant plastic deformations. The first flexural cracks appeared at a load level of 40 kN, which resulted in a decrease in the stiffness as depicted by the slope change in Fig. 6. This was followed by steel yielding and further development of the cracks [Fig. 7(a)], accompanied by large deflections. As expected, all corners of the slab were progressively uplifted as a result of the significant twisting moments [Fig. 8(a)]. Ultimately, the control slab reached a maximum load of 95 kN. At that point the collapse mechanism of the slab involved the formation of an almost circular-shaped crack, which appeared at the top of the slab [marked red in Fig. 8(b)], as a result of moment redistribution at very large displacements.

Slab C1, which was strengthened with one carbon-fiber TRM layer, failed in a similar way (flexure-dominated behavior) but at a substantially higher load, equal to 207 kN, owing to the contribution of the TRM to the flexural resistance. The slab exhibited a stiffer behavior with respect to the control slab (42% increase in the precracking stiffness—see Table 2), and as indicated by the change in the slope of the load-displacement curve in Fig. 6, the cracking

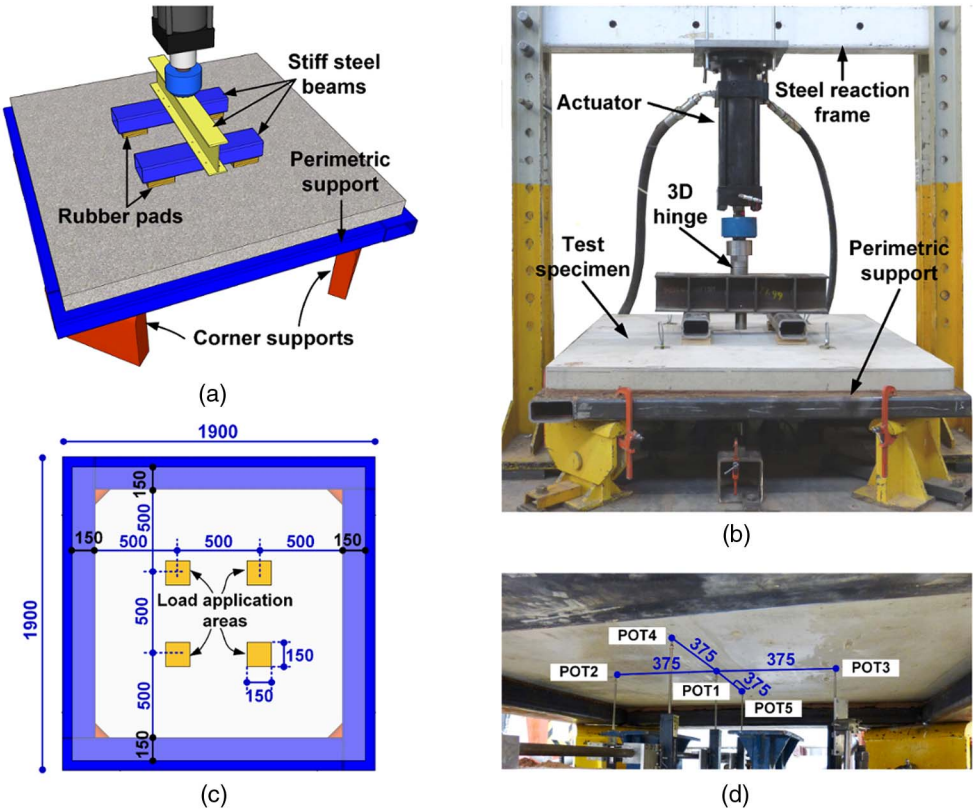

Fig. 5. Test setup: (a) schematic 3D illustration; (b) front view picture; (c) top view dimensioning; (d) location of displacement sensors at the bottom to measure deflections (all dimensions in millimeters)

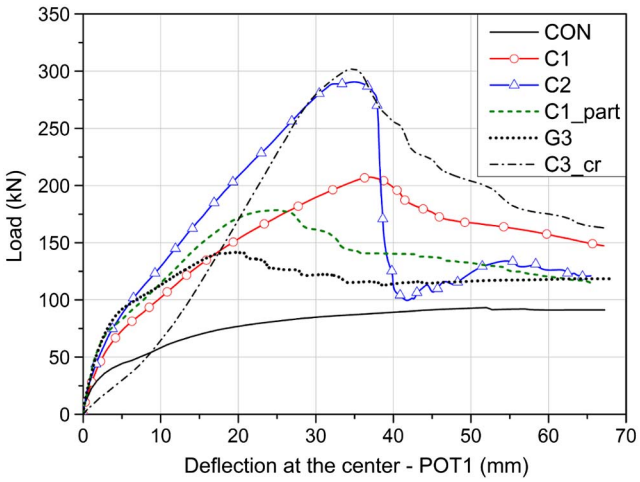

Fig. 6. Load versus central deflection curves

load was also increased, reaching 70 kN. The activation in tension of the fibers crossing the flexural cracks resulted in a significant increase of the postcracking flexural stiffness (4.25 kN/mm) when compared to the CON slab (1.0 kN/mm). The postcracking stiffness in Table 2 has been calculated as the slope between the cracking point and the ultimate load in the load-midspan deflection curves. Fig. 7(b) shows the crack pattern of the C1 slab, which comprises a few major cracks and several minor cracks on the face of the TRM. Failure of this specimen was progressive, as a result of the fibers' partial rupture and slippage within the mortar layer across the major cracks that are visible in Fig. 7(b). After the flexural capacity was reached, the load gradually dropped and a circular-shaped crack appeared at the top of the slab as a part of the collapse mechanism at large displacements, similarly to the CON specimen.

Slab C2, which was strengthened with two carbon-fiber TRM layers, failed at an even higher load, equal to 291 kN, owing to the contribution of the additional carbon TRM layer. The cracking load for this specimen was 90 kN, whereas even higher precracking and postcracking stiffnesses (17.6 and 7.5 kN/mm, respectively) compared to C1 were recorded. Failure of this specimen was attributed to partial slippage of the fibers within the mortar across two cracks [Fig. 7(c)], followed by concrete punching shear [Fig. 8(c)]. The brittle nature of this failure mode resulted in a very abrupt load drop at levels slightly above the ultimate capacity of the CON slab (Fig. 6). The residual capacity was provided by both the steel reinforcement and the TRM layers through the development of a membrane resisting mechanism. The punching area at the top of the slab had a rectangular shape following the perimeter of all four load-application points, indicating that this failure might not have occurred if loading was uniformly distributed.

Slab C1_part, which was strengthened with the same amount of textile reinforcement with slab C1 but in a different configuration (Fig. 2), failed in flexure at an ultimate load of 178 kN. The initial stiffness of this specimen reached even higher levels (24.1 kN/mm) compared to the slabs C1 and C2. The first cracks were developed at a load level of 75 kN, whereas the postcracking stiffness (6.25 kN/mm) was very close to the average of the C1 and C2 slabs' postcracking stiffness (Table 2). This specimen failed in flexure after yielding of the steel reinforcement and slippage of the textile fibers through the mortar, but with a different crack pattern at the face of TRM. As illustrated in Fig. 7(d), four major cracks were

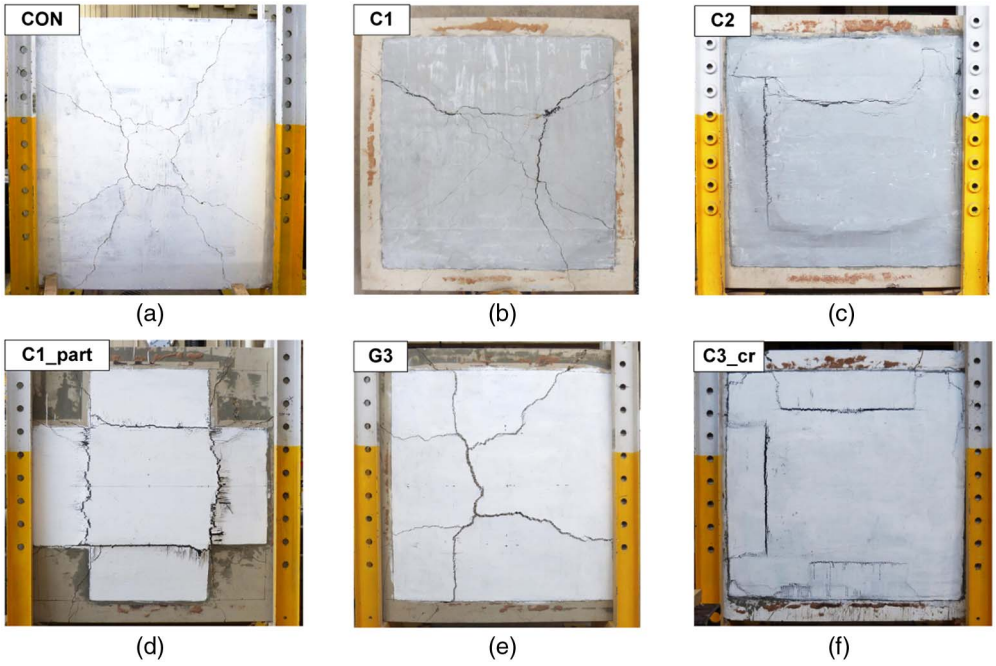

Fig. 7. Crack pattern at the bottom face of tested specimens

Table 2. Summary of Test Results

Specimen	Peak load, P_{max} (kN)	Midspan deflection at P_{max} (mm)	Failure mode	Capacity increase (%)	Precracking stiffness[a] (kN/mm)	Cracking load level[b] (kN)	Postcracking stiffness[a] (kN/mm)	Load at SLS[a] (kN)
CON	95	52	A	—	10.1	40	1.0	47
C1	207	37	B	115	14.3 (42%)	70	4.25 (325%)	79 (68%)
C2	291	35	C	206	17.6 (74%)	90	7.50 (650%)	97 (106%)
C1_part	178	25	B	87	24.1 (139%)	75	6.25 (525%)	89 (89%)
G3	142	20	B	50	22.0 (118%)	90	4.05 (305%)	96 (104%)
C3_cr	302	35	B	218	—	—	10.5 (905%)	—

Note: A = flexural failure; B = slippage and partial rupture of the textile fibers through the mortar followed by flexural failure; C = slippage and partial rupture of the textile fibers through the mortar followed by punching shear failure.
[a]Percentage increase with respect to the CON specimen is included in parenthesis for the retrofitted specimens.
[b]Based on (a) the change in the slope of the load-displacement curve, and (b) test observations.

developed on the face of TRM at the overlapping region of the two strips. The fibers crossing these cracks were highly stressed and ultimately experienced partial rupture and slippage within the mortar, which led to a gradual drop of the load as shown in Fig. 6. The cracks that appeared on the face of the TRM composite did not appear at the location of the cracks developed at the concrete substrate, as revealed in the uncovered part of the slab in Fig. 4(e).

Slab G3, which was strengthened with three layers of glass-fiber TRM, failed in flexure after yielding of the steel reinforcement, at an ultimate load of 142 kN. The initial stiffness of this slab was high enough (22.0 kN/mm), owing to the thickness of the mortar needed for the application of three layers. The load level at first crack was equal to 90 kN, whereas the postcracking stiffness (4.05 kN/mm) was lower than all the other retrofitted slabs. As illustrated in Fig. 7(e), the crack pattern of slab G3 comprised only a few major cracks on the face of the TRM. The failure mode of this specimen is associated with the partial rupture and slippage of the glass fibers within the mortar along the developed cracks [Fig. 8(d)]. This failure mode was identical to that observed in slabs C1 and C1_part and similarly led to a gradual drop of the load.

Finally, specimen C3_cr, which was initially precracked and retrofitted with three layers of carbon-fiber TRM before testing, failed in flexure at a load equal to 302 kN. As shown in Fig. 6, the initial stiffness of this slab was much lower than the stiffness of the rest of the specimens, owing to the cracked state of the concrete. At a load level of 50 kN the stiffness was significantly increased, thus indicating the full activation of the strengthening layers in tension. At this stage, the bending stiffness of slab C3_cr was higher than the stiffness of slab C2 (10.5 kN/mm) as a result of the third TRM layer. Failure was attributed to slippage of the textile fiber within the mortar mainly along the cracks shown in Fig. 7(f).

Discussion of Results

All slabs responded as designed and failed after yielding of the internal steel reinforcement because of the failure (slippage and/or partial fracture) of the externally bonded TRM reinforcement. The flexural capacity of the lightly reinforced concrete slabs was substantially increased by all strengthening schemes proposed in this

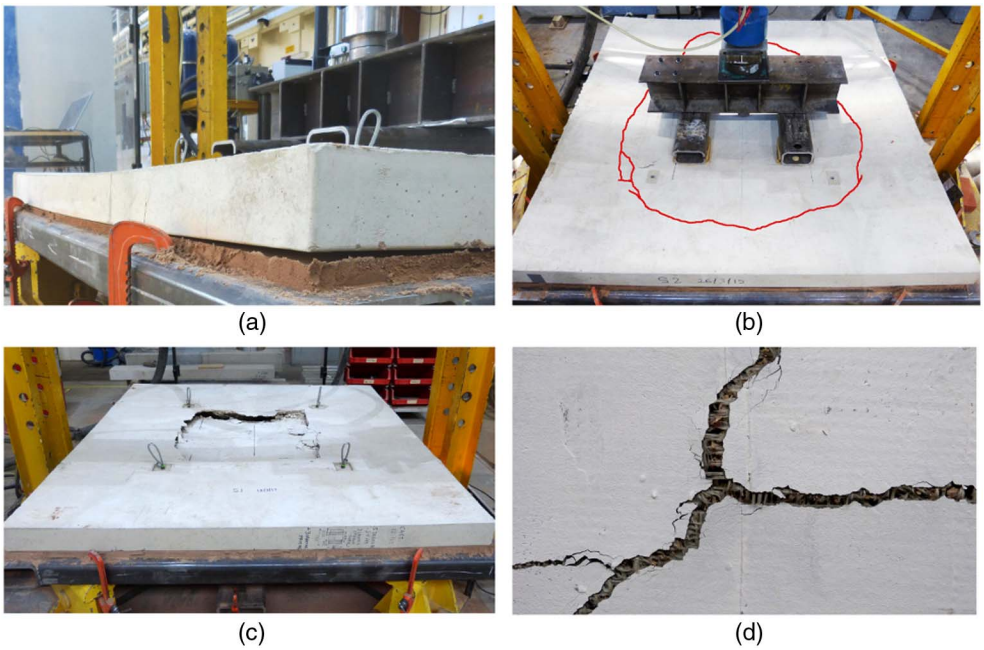

Fig. 8. (a) Corner uplift, CON slab; (b) circular-shaped crack at the top of the CON slab; (c) slab C2 failure in punching shear; (d) partial rupture and slippage of the fibers within the matrix along the cracks on the TRM face, G3 slab

study. In terms of the various parameters investigated in this experimental program, an examination of the results (Table 2) in terms of ultimate capacity, cracking load, precracking (initial) stiffness, postcracking stiffness, and resistance at the serviceability limit state (SLS) revealed the following information.

Number of TRM Layers

A comparison of the results for specimens CON, C1, and C2 shows that the effectiveness of TRM in increasing the flexural capacity of two-way RC slabs was nearly proportional to the number of layers, despite the fact that in specimen C2 punching shear failure ultimately occurred. More specifically, as shown in Table 2, one and two carbon TRM carbon layers resulted in strength increases equal to 115 and 206%, respectively. The increase in the initial stiffness (uncracked stage) was almost proportional to the number of layers (42 and 74% increase for one and two layers, respectively), whereas in terms of postcracking stiffness the increase observed was directly proportional to the number of layers (325 and 650% increase for one and two layers, respectively).

As reported in Table 2, the application of TRM layers in the uncracked slabs increased the flexural resistance at the SLS; this is also illustrated in Fig. 9, which presents the evolution of deflection with the increase of the applied load. By comparing specimens CON, C1, and C2, it is concluded that the flexural resistance at the SLS increases with the number of TRM layers but in a nonproportional way, a 68 and 106% increase for one and two layers, respectively. Similarly, the increase of the cracking load was not proportional, namely 75 and 125% for one and two carbon TRM layers, respectively.

Strengthening Configuration

When specimen C1_part is compared with C1, it is concluded that covering the full face of the slab (with a single textile layer) is more effective in increasing the slab flexural capacity than applying two strips with a half-width in a cross configuration (which are equivalent in terms of the total amount of fibers used and therefore the cost). Nevertheless, if only the fibers in the direction of strengthening application are considered, it is concluded that applying the textile reinforcement close to the region of maximum moments is much more effective. The C1_part specimen having half of the textile reinforcement in each direction with respect to C1 increased the flexural capacity of the slab by 87%, which is nearly 75% of the increase recorded in C1.

The strengthening configuration had a marginal effect on the cracking load increase and the SLS resistance (compared to specimen C1). However, both the initial and the postcracking stiffness increases were substantially higher in the C1_part slab than in C1, by approximately 60 and 70%, respectively. This is attributed to the overlapping of two textile layers in the central maximum moment region (750×750 mm) of the C1_part slab where cracking initiated.

Textile Fibers Material

Three layers of glass textile (which are equivalent to $3/7 = 0.46$ of one layer of carbon textile in terms of axial stiffness) increased the flexural capacity of the slab by 50%, which is 0.43 times the increase for one layer of carbon textile. Therefore, it is concluded that different types of fibers (glass or carbon) show similar effectiveness in terms of the ratio between the load-capacity increase and the axial stiffness of the textile layers. The axial stiffness is expressed by the product of the elastic modulus of the fibers times the thickness of the textile times the number of layers.

The initial stiffness of slab G3 was approximately 50% higher than that of slab C1, whereas the postcracking stiffnesses of these two slabs were very close. Considering that in terms of axial stiffness of the textiles, three layers of glass textile are equivalent to $3/7$ of one layer of carbon textile, the above results indicate that the slab's bending stiffness depends not only on the axial stiffness of the textiles, but also on the total thickness of the TRM jacket. The latter is also believed to be the reason why three layers of glass textiles provided higher cracking load and higher resistance at SLS when compared to one layer of carbon textile.

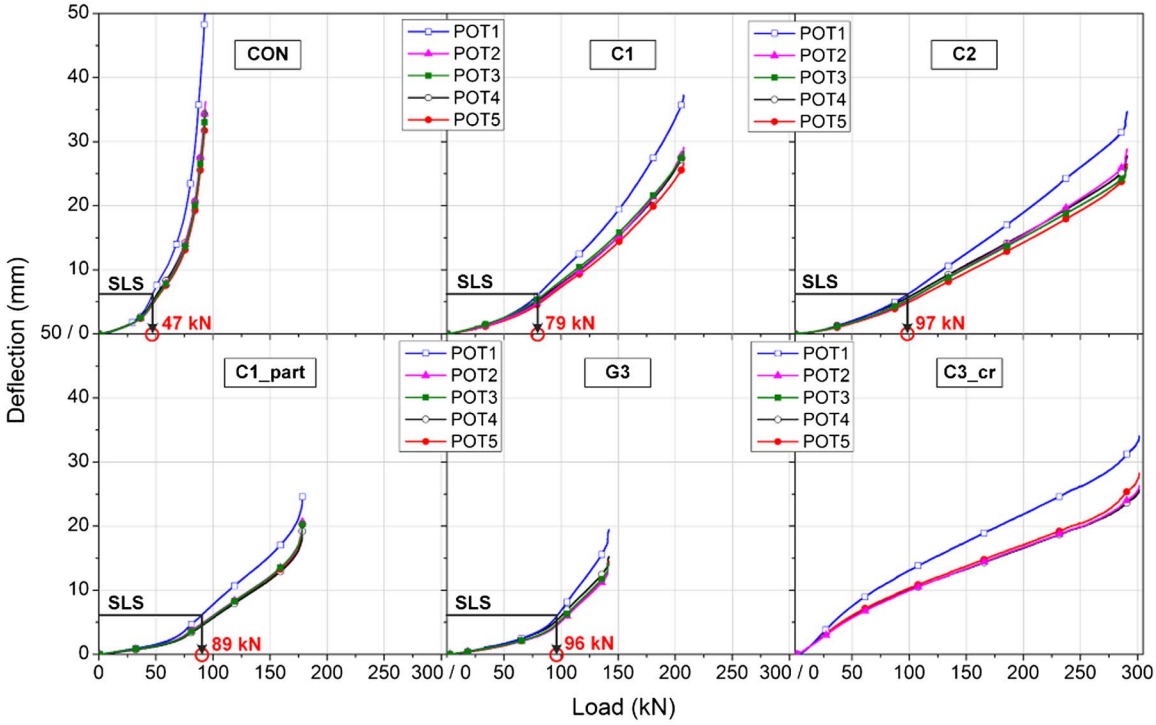

Fig. 9. Deflection evolution at all measuring points with respect to the load increase

Role of Initial Cracking

Despite the reduced effectiveness in increasing the flexural capacity, the precracked slab exhibited the stiffer behavior among all specimens, at the stage where the textile fibers had been fully activated in tension in all slabs (see postcracking stiffness in Table 2). At this stage, the increase in the stiffness was proportional to the number of TRM layers, regardless of the presence of initial cracking or not.

Design Equations

In an attempt to provide simple design equations for calculating the flexural moment of resistance per unit length of two-way slabs retrofitted with TRM, two steps were followed.

Initially, the experimental moment of resistance of the retrofitted slabs was derived after calibrating Eq. (1) to the results of the unretrofitted (CON) slab

$$P_{\max} = k \cdot m_R \tag{1}$$

where $P_{\max}$ = flexural load-bearing capacity; k = load to moment calibration factor; and m_R = flexural moment of resistance per unit length. Through the use of standard cross section analysis-based analytical modeling (Navier-Bernoulli hypothesis for plane cross sections) and the rectangular stress block approach for concrete in compression (without safety factors), the unretrofitted specimen (CON) yielded a value of $m_R = 6.0$ kNm/m. By substituting the ultimate load measured experimentally and the flexural moment of resistance per unit length calculated analytically for the unretrofitted specimen, Eq. (1) yielded a value of k equal to 15.8. This calculated value of k was then used in combination with the peak force of the strengthened specimens (Table 2) to determine the experimental flexural moment of resistance per unit length $m_{R,\exp}$ (second column of Table 3). Note that slab C3_cr was not included in this procedure because of its initial cracked situation.

This approximate approach for defining factor k was deemed necessary because of the lack of reliable analytical models in the literature that correlate the moment of resistance (per unit length) to the applied load in two-way slabs. The value of the k factor, which is commonly derived by applying the so-called yield line theory, is sensitive to the crack (or yield) pattern, which in turn depends on the slab's aspect ratio, the loading and the support conditions. The equation proposed by Rankin and Long (1987) and used also by Ebead and Marzouk (2004) for calculating the flexural capacity of two-way slabs having a crack pattern quite similar to the one observed in this study yielded a value of m_R equal to 11.2 kNm/m. This value underestimates the load-carrying capacity of the unretrofitted slab by 29% and hence it was not further considered for this study.

The effective tensile stress in the TRM reinforcement at flexural failure, f_{te}, was then calculated based on the $m_{R,\exp}$ values, using cross section analysis for the flexurally strengthened slabs, with the tensile force (per unit length), F_t, carried by the TRM layers being expressed by the Eq. (2)

$$F_t = t_t f_{te} \frac{w_t}{w_s} \tag{2}$$

where w_t/w_s = factor to account for the case where the TRM width (w_t) covers only a part of the slab width (w_s), like in the C1_part specimen.

The obtained TRM effective stress and concrete strain values at the ultimate limit state (failure of TRM) are reported in Table 3 as $f_{te,\exp}$ and $\varepsilon_{c,\exp}$, respectively. It is observed that in the case of full coverage of the slab's tensile face with TRM, for textile reinforcement ratios, ρ_t, in the range of 0.095–0.19%, the TRM effective stress varies between 765 and 922 MPa for carbon TRM and is approximately 300 MPa for glass TRM. However, in the case of half coverage of the slab's tensile face with carbon TRM in each direction, a much higher stress value of 1,305 MPa was obtained, indicating better fiber utilization when applied close to the region of

Table 3. Experimental, Theoretical, and Design Values of Flexural Moment Capacity

Specimen	$m_{R,\exp} = P_{\max}/k$ (kNm/m)	$f_{te,\exp}$ (MPa)	$\varepsilon_{c,\exp}$ (‰)	$f_{te,\text{theor}}$ (MPa)	f_{ted} (MPa)	$\varepsilon_{c,\text{theor}}$ (‰)	$m_{R,\text{theor}}$ (kNm/m)	$m_{R,d}$ (kNm/m)	$m_{R,\text{theor}}/m_{R,\exp}$	$m_{R,d}/m_{R,\exp}$
C1	13.2	922	0.95	963	642	1.0	13.8	10.8	1.05	0.82
C2	18.4	765	1.10	727	484	1.0	17.7	13.2	0.96	0.72
C1_part	11.1	1,305	0.95	1,275	850	1.0	11.1	9.1	1.00	0.82
G3	9.0	303	0.75	300	200	1.0	9.1	7.8	1.01	0.87

maximum moments. The concrete strain values were close to 1% in both cases of coverage.

Based on the above findings and with the aim of eliminating the need for iterative calculations and cross section analysis, simple formulas for the calculation of the flexural moment of resistance of slabs retrofitted with TRM are proposed in this study. Following the suggestion of Ebead and Marzouk (2004) for the case of FRP retrofitted slabs, here the moment of resistance per unit length, m_R, can be calculated as the summary of the contribution of the steel reinforcement, m_{Rs}, and the TRM, m_{Rt} [Eq. (3)]

$$m_R = m_{Rs} + m_{Rt} \tag{3}$$

The contribution of the steel reinforcement to the total moment of resistance can be approximately taken equal to the moment of resistance of the unretrofitted slab. Based on the recommendations of ACI 318-08 (ACI 2008), the following simple formula to calculate m_{Rs} (in absence of compression reinforcement) is proposed:

$$m_{Rs} = \rho_s f_y d^2 \left(1 - 0.59 \frac{\rho_s f_y}{f_c}\right) \tag{4}$$

The contribution of the textile reinforcement to the moment of resistance is calculated by Eq. (5)

$$m_{Rt} = F_t \left(h - \frac{x}{2}\right) \tag{5}$$

where F_t is expressed by Eq. (2), and the neutral axis depth, x, is calculated via Eq. (6)

$$x = \frac{\varepsilon_c}{f_{te}/E_f + \varepsilon_c} \tag{6}$$

It is proposed in this study that the value of TRM effective stress (f_{te}) to be used in Eqs. (2) and (6) can be calculated from Eq. (7) for carbon-fiber TRM, whereas for glass fiber TRM a value of $f_{te} =$ 300 MPa should be considered until more experimental data become available. Eq. (7) has been derived by fitting a power equation to the experimental results, considering the different reinforcement ratios of specimens C1, C2, and C1_part (Fig. 10). An upper limit for f_{te} has been set to 1,300 MPa

$$f_{te} = 57.5\rho_t^{-0.405} \leq 1300 \text{ MPa} \tag{7}$$

The value of concrete compressive strain to be used in Eq. (6) is suggested to be $\varepsilon_c = 0.001$ (based on the values of $\varepsilon_{c,\exp}$ in Table 3). A sensitivity analysis showed that the results are not very sensitive to this parameter. For example, by increasing ε_c from 0.005 to 0.0035 (600% increase), m_{Rt} decreases by 20%, whereas for more rational values of ε_c in the range of 0.01 ± 0.005 the m_{Rt} values change from −5.5% to +4.5%.

For design purposes it is recommended to use a design value of the TRM contribution to the moment of resistance, simply by using a design value for the effective stress, f_{ted} (dashed curve in Fig. 10). This value is here suggested to be calculated as

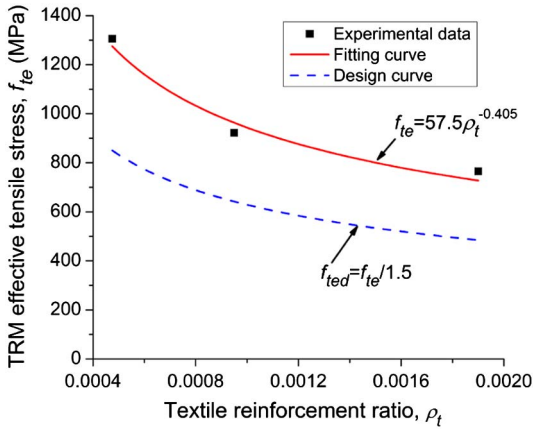

Fig. 10. Fitting of a power equation to the experimental results of specimens C1, C2, and C1_part

$$f_{\text{ted}} = \frac{f_{te}}{1.50} \tag{8}$$

By applying the proposed methodology [Eqs. (1)–(8)], the theoretical values of the flexural moment of resistance, $m_{R,\text{theor}}$ (using f_{te} values), as well as the design values, $m_{R,d}$ (using f_{ted} values), were calculated for the retrofitted slabs tested in this study and are presented in Table 3 (except for the slab C1_cr). The results show very good agreement between the experimental and theoretical values of the flexural moment of resistance. The suggestions for the value of the effective stress that should be used in Eqs. (2) and (6) are based only on the results of this study and therefore should be treated carefully. A refined model should be developed when more experimental data will become available. After obtaining the flexural capacity of the retrofitted slabs, the design engineer should check that it does not exceed the punching shear capacity.

Conclusions

This paper presents an experimental investigation on the effectiveness of a novel material, namely textile-reinforced mortar (TRM), as a means of strengthening in flexure two-way RC slabs. The design of specimens allowed the investigation of a series of parameters including the number of TRM layers, the strengthening configuration, the type of fibers, and the role of initial cracking in the slab. In addition, design equations are suggested, based on the test results. The main conclusions are summarized in a rather qualitative manner as follows:

- The application of TRM layers increased dramatically the flexural capacity of two-way RC slabs. Therefore a viable alternative retrofitting solution, with clear advantages over FRPs, is proposed for the flexural strengthening of deficient two-way RC slabs.

- Increasing the number of TRM layers results in increases in precracking (initial) stiffness, cracking load, postcracking stiffness and ultimate load capacity. The flexural resistance at the serviceability limit state also increases.
- Covering the full face of the slab with a single textile layer is more effective in increasing the flexural capacity than applying two strips with half-width in a cross configuration. Nevertheless, the fibers in the main direction are better activated in the second case, thus resulting in higher strains and postcracking stiffness.
- Different types of fibers (glass or carbon) result in a load capacity increase that is proportional to the axial stiffness of the textile layers.
- The effectiveness of TRM in increasing the flexural capacity two-way slabs is slightly reduced in precracked slabs. However, the increase in postcracking stiffness was found to be proportional to the number of TRM layers, irrespective of the presence of initial cracking.
- Based on the results presented in this study, simple design equations that provide good estimation of the flexural moment of resistance are proposed, eliminating the need for an iterative design procedure.

In view of the limited number of tests performed in this study, the above results as well as the design equations should be considered as rather preliminary. Future research should be directed toward providing a better understanding of parameters, including textile geometry, steel reinforcement ratio, and different slab dimensions, to investigate possible scale effects.

Acknowledgments

The authors wish to thank the students Joshua Spong, Sultan Alotaibi, Saad Raoof, and Zoi Tetta, the lab manager Mike Langford, the chief technician Nigel Rook and the technicians Gary Davies, Sam Cook, and Balbir Loyla, for their assistance in the experimental work. The research described in this paper has been financed by the University of Nottingham through the Dean of Engineering Prize, a scheme for pump priming support for early career academic staff.

Notation

The following symbols are used in this paper:

d = effective depth of the slab;
E_t = TRM elastic modulus taken equal to the fibers' modulus of elasticity;
F_t = tensile force carried by TRM;
f_c = concrete compressive strength;
f_{te} = TRM effective stress value at the ultimate limit state;
f_{ted} = design value of TRM effective stress value at the ultimate limit state;
f_y = steel reinforcement yield stress;
h = section height equal to the slab thickness;
k = load to moment calibration factor;
m_R = flexural moment of resistance per unit length;
m_{Rs} = contribution of the steel reinforcement to the moment of resistance;
m_{Rt} = contribution of the TRM to the moment of resistance;
$P_{\max}$ = flexural load-bearing capacity;
t_t = TRM thickness taken equal to the textile thickness times the number of layers;
w_s = slab width;
w_t = TRM width;
x = depth of neutral axis;
γ_t = safety factor for the TRM contribution to the moment of resistance;
ε_c = concrete compressive strain;
ρ_s = steel reinforcement ratio equal to the steel area per 1 m divided by the effective depth of the slab; and
ρ_t = textile reinforcement ratio equal to the fibers' area per 1 m (per direction) divided by the thickness of the slab (multiplied by the factor w_t/w_s for partially covered slabs).

References

ACI (American Concrete Institute). (2008). "Building code requirements for structural concrete." *ACI 549*, Farmington Hills, MI.

ACI (American Concrete Institute). (2013). "Design and construction guide of externally bonded FRCM systems for concrete and masonry repair and strengthening." *ACI 549*, Farmington Hills, MI.

Babaeidarabad, S., De Caso, F., and Nanni, A. (2013). "URM walls strengthened with fabric-reinforced cementitious matrix composite subjected to diagonal compression." *J. Compos. Constr.*, 10.1061/(ASCE)CC.1943-5614.0000441, 04013045.

Babaeidarabad, S., Loreto, G., and Nanni, A. (2014). "Flexural strengthening of RC beams with an externally bonded fabric-reinforced cementitious matrix." *J. Compos. Constr.*, 10.1061/(ASCE)CC.1943-5614.0000473, 04014009.

Bournas, D. A., Lontou, P., Papanicolaou, C. G., and Triantafillou, T. C. (2007). "Textile-reinforced mortar versus fiber-reinforced polymer confinement in reinforced concrete columns." *ACI Struct. J.*, 104(6), 740–748.

Bournas, D. A., Pavese, A., and Tizani, W. (2015). "Tensile capacity of FRP anchors in connecting FRP and TRM sheets to concrete." *Eng. Struct.*, 82(1), 72–81.

Bournas, D. A., and Triantafillou, T. C. (2011). "Bond strength of lap-spliced bars in concrete confined with composite jackets." *J. Compos. Constr.*, 10.1061/(ASCE)CC.1943-5614.0000078, 156–167.

Bournas, D. A., Triantafillou, T. C., Zygouris, K., and Stavropoulos, F. (2009). "Textile-reinforced mortar versus FRP jacketing in seismic retrofitting of RC columns with continuous or lap-spliced deformed bars." *J. Compos. Constr.*, 10.1061/(ASCE)CC.1943-5614.0000028, 360–371.

Brameshuber, W., eds. (2016). "Textile reinforced concrete, state-of-the-art report of RILEM technical committee 201-TRC." *RILEM Rep. 36*, RILEM, Bagneux, France.

Carloni, C., et al. (2015). "Fiber reinforced composites with cementitious (inorganic) matrix." *Design procedures for the use of composites in strengthening of reinforced concrete structures—State of the art report of the RILEM TC 234-DUC*, C. Pellegrino and J. Sena-Cruz, eds., Springer, Netherlands, 349–391.

CEN (European Committee for Standardization). (1999). "Methods of test for mortar for masonry—Part 11: Determination of flexural and compressive strength of hardened mortar." *EN 1015-11*, Brussels, Belgium.

CEN (European Committee for Standardization). (2004). "Eurocode 2: Design of concrete structures—Part 1: General rules, seismic actions and rules for buildings." *EN 1992-1-1*, Brussels, Belgium.

D'Ambrisi, A., and Focacci, F. (2011). "Flexural strengthening of RC beams with cement-based composites." *J. Compos. Constr.*, 10.1061/(ASCE)CC.1943-5614.0000218, 707–720.

Ebeaed, U., and Marzouk, H. (2004). "Fiber-reinforced polymer strengthening of two-way slabs." *ACI Struct. J.*, 101(5), 650–659.

Elsanadedy, H., Almusallam, T., Alsayed, S., and Al-Salloum, Y. (2013). "Flexural strengthening of RC beams using textile reinforced mortar—Experimental and numerical study." *Compos. Struct.*, 97, 40–55.

Harajli, M., El Khatib, H., and San-Jose, J. T. (2010). "Static and cyclic out-of-plane response of masonry walls strengthened using textile-mortar system." *J. Mater. Civ. Eng.*, 10.1061/(ASCE)MT.1943-5533.0000128, 1171–1180.

Jesse, F., Weiland, S., and Curbach, M. (2008). "Flexural strengthening of RC structures with textile-reinforced concrete." *Am. Concr. Inst.*, 250, 49–58.

Koutas, L., Bousias, S. N., and Triantafillou, T. C. (2015a). "Seismic strengthening of masonry-infilled RC frames with TRM: Experimental study." *J. Compos. Constr.*, 10.1061/(ASCE)CC.1943-5614.0000507, 04014048.

Koutas, L., Pitytzogia, A., Triantafillou, T. C., and Bousias, S. N. (2014). "Strengthening of infilled reinforced concrete frames with TRM: Study on the development and testing of textile-based anchors." *J. Compos. Constr.*, 10.1061/(ASCE)CC.1943-5614.0000390, A4013015.

Koutas, L., Triantafillou, T. C., and Bousias, S. N. (2015b). "Analytical modeling of masonry-infilled RC frames retrofitted with textile-reinforced mortar." *J. Compos. Constr.*, 10.1061/(ASCE)CC.1943-5614.0000553, 04014082.

Loreto, G., Babaeidarabad, S., Leardini, L., and Nanni, A. (2015). "RC beams shear-strengthened with fabric-reinforced-cementitious-matrix (FRCM) composite." *Int. J. Adv. Struct. Eng.*, 7(4), 341–352.

Loreto, G., Leardini, L., Arboleda, D., and Nanni, A. (2014). "Performance of RC slab-type elements strengthened with fabric-reinforced cementitious-matrix composites." *J. Compos. Constr.*, 10.1061/(ASCE)CC.1943-5614.0000415, A4013003.

Ombres, L. (2015). "Structural performances of reinforced concrete beams strengthened in shear with a cement based fiber composite material." *Compos. Struct.*, 122, 316–329.

Papanicolaou, C., Triantafillou, T., Papantoniou, I., and Balioukos, C. (2009). "Strengthening of two-way reinforced concrete slabs with textile reinforced mortars (TRM)." *Proc., 4th Colloquium on Textile Reinforced Structures (CTRS4)*, M. Curbach and F. Jesse, eds., Dresden, Germany, 409–420.

Papanicolaou, C. G., Triantafillou, T. C., Karlos, K., and Papathanasiou, M. (2007). "Textile-reinforced mortar (TRM) versus FRP as strengthening material of URM walls: In-plane cyclic loading." *Mater. Struct.*, 40(10), 1081–1097.

Rankin, G. I. B., and Long, A. E. (1987). "Predicting the punching strength of conventional slab-column specimens." *Proc. Inst. Civ. Eng.*, 82(2), 327–346.

Schladitz, F., Frenzel, M., Ehlig, D., and Curbach, M. (2012). "Bending load capacity of reinforced concrete slabs strengthened with textile reinforced concrete." *Eng. Struct.*, 40, 317–326.

Tetta, Z. C., Koutas, L. N., and Bournas, D. A. (2015). "Textile-reinforced mortar (TRM) versus fiber-reinforced polymers (FRP) in shear strengthening of concrete beams." *Compos. Part B*, 77, 338–348.

Tetta, Z. C., Koutas, L. N. and Bournas, D. A. (2016). "Shear strengthening of full-scale RC T-beams using textile-reinforced mortar and textile-based anchors." *Compos. Part B*, 95, 225–239.

Triantafillou, T. C., Papanicolaou, C. G., Zissimopoulos, P., and Laourdekis, T. (2006). "Concrete confinement with textile-reinforced mortar jackets." *ACI Struct. J.*, 103(1), 28–37.

Tzoura, E., and Triantafillou, T. C. (2014). "Shear strengthening of reinforced concrete T-beams under cyclic loading with TRM or FRP jackets." *Mater. Struct.*, 49(1–2), 17–28.